Phytomedicine 135 (2024) 156119

Contents lists available at ScienceDirect

Phytomedicine

journal homepage: www.elsevier.com/locate/phymed

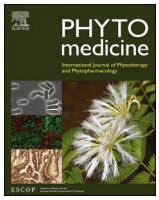

Original Article

Alizarin attenuates oxidative stress-induced mitochondrial damage in vascular dementia rats by promoting TRPM2 ubiquitination and proteasomal degradation via Smurf2

Guo-pin Pan [a], Yan-hua Liu [a,b], Ming-xu Qi [c], Ya-qi Guo [a], Zhen-lei Shao [a,b], Hui-ting Liu [a], Yi-wen Qian [d], Shuang Guo [e], Ya-ling Yin [a,*], Peng Li [a,*]

[a] Henan international joint laboratory of cardiovascular remodeling and drug intervention, Sino-UK Joint Laboratory of Brain Function and Injury and Department of Physiology and Neurobiology, School of Basic Medical Sciences, College of Pharmacy, Xinxiang Medical University, Xinxiang 453003, China
[b] Pharmacy Department, the First Affiliated Hospital, Xinxiang Medical University, Xinxiang 453003, China
[c] College of Pharmacy, Changchun University of Chinese Medicine, Changchun 130000, China
[d] Department of Pharmacy, College of Basic Medicine and Forensic Medicien, Henan University of Science and Technology, Luoyang 471000, China
[e] Hubei Key Laboratory of Diabetes and Angiopathy, Hubei University of Science and Technology, Xianning 437100, China

ARTICLE INFO

Keywords:
Oxidative stress
Alizarin
Vascular dementia
TRPM2
Smurf2
Ubiquitination

ABSTRACT

Background: Alizarin (AZ) is a natural anthraquinone with anti-inflammatory and moderate antioxidant properties.
Purpose: In this study, we characterized the role of AZ in a rat model of vascular dementia (VaD) and explored its underlying mechanisms.
Methods: VaD was induced by bilateral common carotid artery occlusion.
Results: We found that AZ attenuated oxidative stress and improved mitochondrial structure and function in VaD rats, which led to the improvement of their learning and memory function. Mechanistically, AZ reduced transient receptor potential melastatin 2 (TRPM2) expression and activation of the Janus-kinase and signal transducer activator of transcription (JAK-STAT) pathway in VaD rats. In particular, the reduction in the expression of TRPM2 channels was the key to the attenuation of the oxidative stress-induced mitochondrial damage, which may be achieved by increasing the expression of the E3 ubiquitin ligase, Smad-ubiquitination regulatory factor 2 (Smurf2); thereby increasing the ubiquitination and degradation levels of TRPM2.
Conclusion: Our results suggest that AZ is an effective candidate drug for ameliorating VaD and provide new insights into the current clinical treatment of VaD.

Introduction

Vascular dementia (VaD) is a degenerative cerebrovascular disease with progressive cognitive decline and impaired functional autonomy caused by cerebrovascular disease or cardiovascular pathology (Yang et al., 2022). VaD is considered the second most common type of senile dementia after Alzheimer's disease (Kalaria, 2018) . The increasing aging population and surge in cardiometabolic risk factors have made VaD a serious public health problem (Romay et al., 2019). Despite ongoing research into pharmacologic and non-pharmacologic treatments (Bordet et al., 2017), to date no approved symptomatic treatments are available for VaD (Erkinjuntti et al., 2004; O'Brien and Thomas, 2015), and the efficacy of existing symptomatic therapies is not satisfactory (Korczyn et al., 2012). Therefore, understanding the pathogenesis of VaD and developing methods for its prevention and treatment are top clinical priorities.

Abbreviations: AZ, Alizarin; VaD, vascular dementia; TRPM2, transient receptor potential melastatin 2; JAK/STAT, the Janus-kinase and signal transducer activator of transcription; ROS, reactive oxygen species; TNFα, tumor necrosis factor alpha; SD, Sprague-Dawley; 2VO, 2-vessel occlusion; MWM, Morris water maze; H&E, hematoxylin and eosin; DHE, dihydroethidium; mNGF, mouse nerve growth factor; SD, standard deviation; ANOVA, analysis of variance; GSH, reduced glutathione; MDA, malondialdehyde; SOD, superoxide dismutase; NOX, NADPH oxidase; Drp1, dynamin-related protein 1; FIS1, fission protein 1; Smurf2, Smad-ubiquitination regulatory factor 2; PI3-K, phosphatidylinositol 3-kinase; ERK1/2, extracellular signal-regulated kinase; NO, nitric oxide.

* Corresponding authors.
E-mail addresses: yalingyin@xxmu.edu.cn (Y.-l. Yin), pengli@xxmu.edu.cn (P. Li).

https://doi.org/10.1016/j.phymed.2024.156119
Received 22 March 2024; Received in revised form 27 June 2024; Accepted 13 July 2024
Available online 5 October 2024

Mitochondrial damage owing to cellular energy depletion and oxidative stress is associated with cognitive dysfunction and VaD (Fivenson et al., 2017; Lanza et al., 2018). Oxidative stress is a key feature of cerebral ischemic diseases, and oxidative stress and microvascular inflammation play important roles in VaD pathogenesis (Yang and Zhang, 2021). Following vascular injury-induced cerebral ischemia, alterations in circulating glucose levels raise reactive oxygen species (ROS) levels, which promote oxidative stress (Warren et al., 2014). Elevated ROS levels exacerbate vascular endothelial damage and dysfunction (Chrissobolis et al., 2012; Gray and Jandeleit-Dahm, 2015). Thus, an ROS imbalance is directly related to the development of dementia (Bennett et al., 2009). Consistent with this, brains with vascular injury have high levels of free radicals. Cerebral hypoperfusion is also associated with mitochondrial dysfunction and bioenergetic failure, which are recognized as early signs of neurodegenerative disorders, such as VaD (Esteras et al., 2016). For example, tight junction production is highly dependent on mitochondrial metabolism, and a dysfunctional neurovascular unit predisposes neuronal dysfunction and apoptosis (Parodi-Rullán et al., 2019). Metabolism and ROS production in the mitochondria are tightly interconnected, such that failure of the electron transport chain and oxidative phosphorylation leads to excessive mitochondrial ROS production. High and sustained ROS levels impair mitochondrial function and promote hypoxia and cell death (Venkat et al., 2015). A tumor necrosis factor alpha (TNFα) antagonist has been reported to partially restore neurovascular function, suggesting that targeting oxidative stress and inflammation may be a promising strategy for the treatment of VaD (Finger et al., 2022).

Alizarin (AZ) (1,2-dihydroxyanthraquinone) is the most active anthraquinone isolated from the roots of alizarin (Xu et al., 2020) in its glycosidic form, possesses a wide range of biological effects, and has recently gained much attention. On the one hand, anthraquinones are molecules with a moderate antioxidant capacity (Cai et al., 2006). AZ inhibits the proliferation of osteosarcoma and breast cancer cells by inhibiting the phosphorylation of extracellular signal-regulated kinases (ERK) (Fotia et al., 2012). In vivo and in vitro experiments indicated the capacity of AZ to act as a scavenger of free radicals (Cai et al., 2006; Jeremić et al., 2018). On the other hand, anthraquinone compounds have a variety of pharmacological activities, including anti-inflammatory, antimicrobial, anticancer, ameliorating lipid metabolism abnormalities, and antiplatelet activities (Cai et al., 2006; Fuentes et al., 2018; Nam et al., 2017). AZ has been used to treat various diseases, including Alzheimer's disease, diabetes, cancer, acne, inflammation, allergies, small bowel colitis, and bacterial and viral infections (Cai et al., 2004). Other reported applications include immunomodulator, analgesic, diuretic, gastroprotector, hepatoprotector, and nephroprotector (Cai et al., 2004). A recent study by our group found that AZ improved cardiac dysfunction and attenuated myocardial injury in diabetic cardiomyopathy rats by reducing oxidative stress and controlling blood glucose level (Zhu et al., 2023). Despite attempts to use AZ in Alzheimer's, its neuroprotective effects have not been fully recognized, which may be related to the fact that anthraquinone compounds effectively inhibit amyloid aggregation (Convertino et al., 2009). However, the effect of AZ on VaD has rarely been reported.

The transient receptor potential melastatin 2 (TRPM2) is a voltage-independent, Ca^{2+}-permeable nonselective cation channel that is highly sensitive to oxidative stress (Malko and Jiang, 2020) and is activated by oxidants, such as hydrogen peroxide. Activated TRPM2 induces a sustained increase in intracellular calcium-free ion concentration ($[Ca^{2+}]i$) and activates the inflammatory response (Alves-Lopes et al., 2020; Li and Jiang, 2019), eventually inducing cell death (Ramsey et al., 2006). TRPM2 is widely expressed in the central nervous system (Bai and Lipski, 2010) and is involved in the pathogenesis of neurodegenerative diseases (Xie et al., 2010), cardiovascular diseases (Zielińska et al., 2021), and various cancers (Miller, 2019). TRPM2 channels may be central to the integration of oxidative stress, calcium dysregulation, and mitochondrial dysfunction (Freestone et al., 2009). Previous studies by our group found that reduced TRPM2 is associated with improved cognitive function in rats with vascular dementia (Qiu et al., 2021; Yin et al., 2022).

The present experimental study aimed to determine whether AZ is effective in improving cognitive function in VaD rats by attenuating oxidative stress-induced mitochondrial damage via TRPM2 and to elucidate the specific mechanism.

Materials and methods

Major reagent

AZ (≥99 % purity) was purchased from Lanabai Pharmaceutical & Chemical Co., Ltd. (wuhan, China). The chemical structure of AZ was shown in the supplementary Fig.S1. Mouse Nerve Growth Factor (mNGF) for injection was obtained from Sinobioway Biomedicine Co., Ltd. (production batch number: 20,190,702). Dihydroethidium (DHE) fluorescent probe kit was purchased from Abcam. MG132 was purchased from MCE (Cat. No.: HY-13,259).

The following primary antibodies were used: TRPM2 (ab11168, abcam), Smurf2(#12,024) and p-STAT2 (Tyr690, #88,410) are from Cell Signaling Technology; JAK1(Cat No: 66,466-1-Ig), Drp1(Cat No: 12,957-1-AP), FIS1(Cat No: 10,956-1-AP), VDAC1(Cat No: 55,259-1-AP), NOX2(Cat No: 19,013-1-AP), NOX4(Cat No: 14,347-1-AP) are from Proteintech (Wuhan, China), FLAG and GAPDH (Sigma); HA and Myc (Santa Cruz).

Animals and experimental designs

Male Sprague-Dawley (SD) rats (180 ± 20 g) and C57BL/6 J (TRPM2 wild-type,$TRPM2^{+/+}$, 25 ± 5 g) mice were purchased from the Experimental Animal Center of Zhengzhou University (Henan, China, license number: SYXK-Yu-2014–0005). TRPM2 knockout mice ($TRPM2^{-/-}$) (8 weeks, 25 ± 5 g) were provided by Professor Jiang Lin-Hua. All animals were housed in cages with room temperature of 22 °C −24 °C with a 12 h light/dark cycle. Food and water were provided ad libitum. The animal experiments in this study were approved by the Animal Care Committee of Xinxiang Medical University (No:XYLL-2022YY857, fourth Nov.,2022) . Animals were handled in accordance with the National Institutes of Health guide for the care and use of laboratory animals (NIH Publications No 8023, revised 1978).

After one week of acclimatization feeding, rats were randomly divided into eight groups: (a) Control group (Con) , (b) AZ (25 mg kg^{-1}/day)group, (c) VaD group, (d) VaD + AZ (l) (2.5 mg kg^{-1}/day) group, (e) VaD + AZ (M) (8 mg kg^{-1}/day) group, (f) VaD + AZ (H) (25 mg kg^{-1}/day) group, (g) VaD + mNGF (2 μg/kg/day) group, (h) VaD + AZ (25 mg kg^{-1}/day)+ mNGF (2 μg/kg/day) group (n = 8 each group) . The first two groups of rats were fed with conventional chow, and the latter six groups were treated with bilateral common carotid artery occlusion (2-vessel occlusion,2VO) to establish vascular dementia model. After 4 weeks, neurological function tests and water maze experiments were performed to determine whether the modeling was successful. After the VaD model was successfully established, AZ or mNGF was given for treatment for 4 weeks (AZ by gavage and mNGF by intraperitoneal injection). Animals were sacrificed after behavior test and the hippocampal tissues of animals were separated for morphological analysis. The dosage and route of administration of AZ were referred to our previous study (Zhu et al., 2023) and experiments with different doses were done.

In addition, $TRPM2^{+/+}$ and $TRPM2^{-/-}$mice were randomly divided into two groups respectively (n = 10, per group): $TRPM2^{+/+}$+2VO group, $TRPM2^{+/+}$+2VO +AZ group and $TRPM2^{-/-}$ +2VO group, $TRPM2^{-/-}$+2VO +AZ group (40 mg kg^{-1}/day, gavage for 4 weeks). The $TRPM2^{+/+}$ and $TRPM2^{-/-}$ group mice were fed with daily feeding.

VaD model induction

The VaD model was performed using 2VO according to the protocol described previously (Qiu et al., 2021; Yin et al., 2022). Briefly, rats (mouse) were fasted for 12 h before surgery and anesthetized by intraperitoneal injection of sodium pentobarbital 60 mg kg^{-1} (30 mg kg^{-1} for mouse) . Bilateral common carotid arteries were ligated with 5–0 silk thread. Postoperative penicillin was injected intramuscularly for 3 days to prevent infection.

Morris water maze (MWM) test

As mentioned earlier, the Morris water maze test (MWM) is used for behavioral assessment of learning and memory (Qiu et al., 2021; Yin et al., 2022). Briefly, the experiment consisted of two phases: training phase and probe test phase. The first 6 days were the training phase, which was conducted twice a day at 20-min intervals. The rats were gently placed into the water in the order of east, west, south and north, with their heads facing the side wall of the maze. The swimming path of the rats was monitored by a video camera connected to a computer via an image analyzer (Columbus Instruments, USA), and the delay time and path length of the escape to the hidden platform were recorded. Rats were given up to 60 s to find the hidden platform. If the rat failed to find the platform within 60 s, the training was terminated and the rat was then guided to the hidden platform for 10 s (Li et al., 2017). The probe test was performed the day after the training phase and the hidden platform was removed. The rats were allowed to swim freely in the pool for 60 s. The rats' swimming trajectories were recorded and the swimming distance, time and speed were analyzed as the assessment of spatial memory.

HE staining

Rats were euthanized by intraperitoneal injection of pentobarbital sodium (~300 mg kg^{-1}) and then perfused with PBS and 4 % paraformaldehyde. The entire brain was excised and fixed in 4 % paraformaldehyde for 24–48 h. Brain segments of the hippocampus were removed and paraffin-embedded after dehydration. Sections of 4-μm thick were cut using a microtome (Leica RM2135, Nussloch, Germany) and stained with hematoxylin and eosin. Images were captured with digital pathology slide scanner (3DHISTECH, Pannoramic SCAN, EU).

Golgi staining

Golgi staining was performed according to the protocol described previously (Qiu et al., 2021). Breifly, hippocampal tissues were cut into 80 μm thick slices at - 20 ~ - 22 °C using a cryosectioner. The sections were stained with Golgi staining kit (Hito Golgi-Cox Optimstain kit, Hitobiotec, USA) according to the instructions. The sections were sealed with neutral gum and then dried at room temperature. The number of dendritic spines and morphology of neurons were observed.

Electron microscope quantitative analysis

The ultrastructure and morphology of neuron mitochondria were observed by electron microscope. Briefly, hippocampus-containing brain tissue was cut into 1-mm-thick pieces and immediately fixed with 2.5 % glutaraldehyde. The ultrathin sections were then examined and imaged using a JEM-1400plus transmission electron microscope (Japan Electro-Optical Laboratories, Inc., Tokyo). Thirty cell fields were taken from each group of specimens, and mitochondria and nuclei were tracked separately for each image using a cursor. The mitochondrial area and aspect ratio (the ratio of length/width) were quantified by ImageJ. Based on their volume ratios in 3D space, the corresponding secondary parameters such as volume density (Vv), shape factor (PE), mean area (S) and mean perimeter (l) were calculated.

Detection of mitochondrial membrane potential

Mitochondrial membrane potential was detected using the Mitochondrial Membrane Potential Assay Kit (Beyotime). JC-1 dye was added to the sections and the sections were visualized at the end of the incubation. Samples were evaluated using Image-Pro Plus 7 software (Media Cybernetics Inc., Rockville, MD, USA).

Detection of ROS by DHE STAining

DHE staining was used to detect ROS. Briefly, sections were incubated with 5 μM DHE for 1 hour at room temperature, and a digital HISTECH (3D HISTECH, Pannoramic SCAN, EU) was used for photography and quantification.

Primary hippocampal neuron culture and treatment

Primary hippocampal neuron culture preparation was processed as described previously (Qiu et al., 2021). In brief, the hippocampus was dissected from a fetal rat, washed in Hank's buffered saline and gently minced. Digestion of the hippocampus with 0.25 % trypsin (Invitrogen) until the final concentration of trypsin was 0.125 %, then the digestion was terminated. The dissociated cell suspension was inoculated into polylysine-coated cell culture plates or dishes for culture. After cell sedimentation, neurons were maintained in a humidified incubator at 37 °C and 5 % CO_2 atmosphere with neuronal medium. Neuronal damage was induced with H_2O_2 (200 μM, 12 h).

When the concentration of AZ was in the range of 5–20 μM, the survival rate of primary neuronal cells were higher than 95 %, which could be regarded as no significant cytotoxicity; therefore, the dosage of AZ used was 20 μM.

siRNA-mediated Gene silencing

The siRNA constructs targeting rat TRPM2 gene was obtained from GenePharma (Shanghai, China). A universal non-targeting sequence was used as control siRNA. Transfection of siRNA was carried out using Lipofectamine 3000 reagent (Thermo Fisher), according to the manufacturer's instructions. Briefly, siRNA and Lipofectamine™ 3000 reagents were mixed in Opti-MEM medium (Invitrogen) and incubated for 30 min at room temperature to allow the complex formation. The siRNA was used at a final concentration of 0.1–0.5 μM 6 h after transfection, cells were washed and changed to fresh medium and further cultured for 2 days before subsequent experimentations.

Immunofluorescence and confocal laser scanning

Brain tissue sections and cells were stained for immunofluorescence as described previously (Qiu et al., 2021). Tissue sections and cells were sealed with 5 % bovine serum albumin for 30 min, then primary antibody was added dropwise and incubated overnight at 4 °C. On the following day, after PBST washing, fluorescent secondary antibodies were incubated for 2 h at room temperature, all images were collected after 4′,6′-diamino-2-phenylindole (DAPI) staining. HA-TRPM2 and Myc-Smurf2 were co-transfected with neurons, and co-localization was observed by laser scanning confocal microscopy.

Western blot assay

Total proteins of hippocampal tissue were extracted using RIPA lysis buffer containing Protein Phosphatase Inhibitors cocktail and phenylmethanesulfonyl fluoride (all from Solarbio). Samples were boiled in SDS sample buffer (62.5 mM Tris–HCl, pH 6.8, 2 % SDS, 10 % glycerol, 5 % 2-mercaptoethanol and 0.02 % bromophenol blue) and separated by 10 % SDS-PAGE and transferred to polyvinylidene fluoride membrane. Membranes were blocked with 5 % non-fat milk, incubated overnight

with primary antibodies at 4 °C on an orbital shaker. After washed three times for 15 min, the membranes were incubated with horseradish peroxidase-conjugated secondary antibodies for 1 hour at room temperature. Immobilon ECL Substrate Kit was used for luminescence development. Images of proteins were visualized using enhanced chemiluminescence kit (Thermo, USA) and densitometry analysis was performed with ImageJ (National Institutes of Health, USA).

Co-immunoprecipitation

Co-immunoprecipitation of Smurf2 and TRPM2 was performed as described previously (Adhikary et al., 2016). Briefly, cells were lysed in lysis buffer, followed by overnight incubation with appropriate primary antibodies and incubation with protein G-agarose beads (Santa Cruz) for 2 h at 4 °C. The beads were washed 3 times with lysis buffer. Bead-bound proteins were mixed with 4X loading dye containing 10 % β-mercaptoethanol. SDS-PAGE was used to separate the proteins and Western blotting was used to analyze cell lysates and immunoprecipitates.

His tag pulldown assay

His-pulldown assays were performed according to the manufacturer's instructions of his-tag isolation and pulldown dynabeads (Invitrogen, Carlsbad, CA). Briefly, HA-TRPM2, His-ubiquitin, and Myc-Smurf2 were co-transfected into mouse primary neurons. The magnetic bead/protein complexes were then washed and resuspended in pull-down buffer (3.25 mM sodium phosphate, 70 mM NaCl and 0.01 % Tween-20). After washing, the eluted proteins were analyzed by SDS-PAGE and western blot.

Determination of relevant oxidation indexes in serum of rats

Plasma samples were extracted from peripheral blood by centrifugation at 550 g for 10 min, and dispensed for the test. Assays were performed according to the manufacturer's instructions of each commercial kit (Nanjing Jiancheng) to detect the content of glutathione (GSH),malondialdehyde (MDA),NADPH and SOD activity.

Statistical analysis

The data are summarized as the means ±standard deviation (SD) using Prism software (GraphPad, San Diego, CA, USA). Statistical analyses included: unpaired *t*-test for comparisons between 2 groups; one-way analysis of variance (ANOVA) followed by post hoc Tukey's test was used to compare multiple groups. Data without a Gaussian distribution were log transformed before statistical analysis. *P* values of <

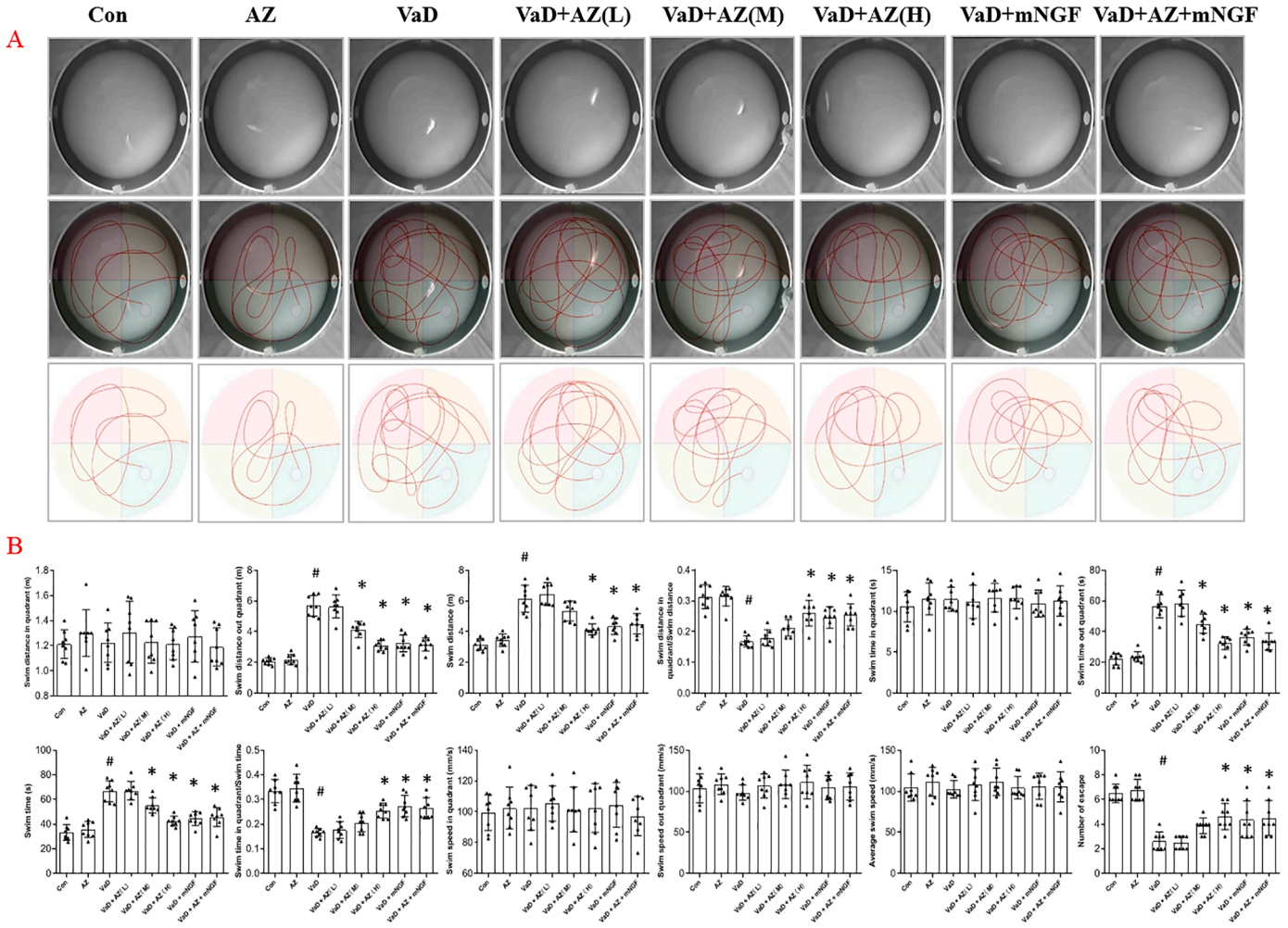

Fig. 1. Effects of AZ on spatial learning and memory in rats with VaD. (A) The trajectory of rats in each group reaching the platform in the swimming pool. (B) Statistics of swim distance in quadrant, swim distance out quadrant, total swim distance, swim distance in quadrant/swim distance, swim time in quadrant, swim time out quadrant, total swim time, swim time in quadrant/swim time, swim speed in quadrant, swim speed out quadrant, average swim speed, number of escape of rats in each group.
Data are reported as mean ± SD. $n = 8$ in each group. #$p < 0.05$ vs Con group; *$p < 0.05$ vs VaD group, one-way ANOVA.

0.05 (two-tailed) were considered as statistically significant. The *n* number represented the number of independent samples but not technical replicates or the selected multiple microscopic fields in each slide (for immunofluorescence assays). For all in vivo studies, the specific group size was pre-determined, and the pre-determined group size was retained by adding replacement animals in the affected group. For in vitro assays, the *n* number was maintained ≥ 3 and equal for all groups unless indicated separately.

Results

AZ improves memory function in rats with VaD

VaD is characterized by a progressive decline in memory and cognition, leading to impaired functional autonomy (Romay et al., 2019). We first used the MWM to observe whether AZ could improve the learning memory ability of VaD rats. The motion trajectories of rats in each group reaching the swimming pool platform were shown in Fig. 1A. During the first 4 days of training, rats in all groups gradually learned to find the hidden platform and shortened the avoidance latency. However, during the second 2 days of the training phase, rats in the VaD group began to show a significant prolongation of the avoidance latency (results not presented). During the recording phase of the probe test, rats in the VaD group showed a significant increase in the mean avoidance latency to find the hidden platform ($p < 0.05$) and a significant decrease in the learning memory ability compared with the control group. Both AZ and mNGF interventions shortened the escape latency and increased the four-quadrant in-swimming distance, the ratio of the four-quadrant in-swimming distance to the four-quadrant out-swimming distance, four-quadrant in-swimming time, the ratio of the four-quadrant in-swimming time to total swimming time, and the escape times (Fig. 1B). While there was no significant difference in total swimming distance and swimming speed among all groups. In addition, we found that the effect of AZ was dose-dependent, and the effect of high-dose AZ intervention was comparable to that of mNGF intervention, and there was no synergistic effect of high-dose AZ and nerve growth factor. The above results preliminarily suggested us that AZ could independently improve spatial learning and memory deficits in VaD rats, without affecting motor function.

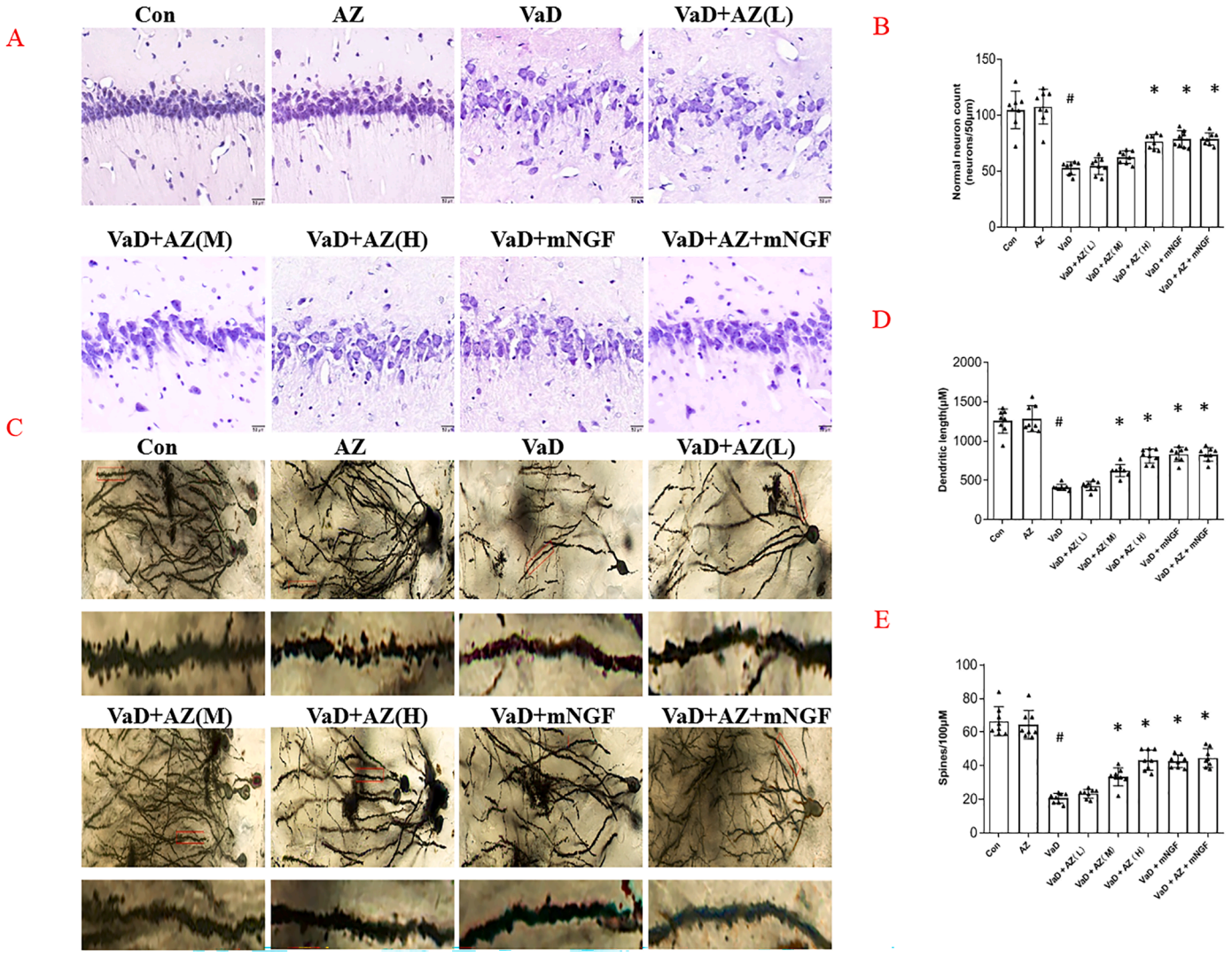

Fig. 2. AZ improved the morphology and structure of hippocampal neurons in VaD rats. (A) the morphology of hippocampus was analyzed by HE staining. (B) Quantitative data showing the number of normal neurons (neurons/50 μm). (C) Golgi-stained neuronal profiles of hippocampus in each group. (D) The quantitative analysis of the dendritic length and (E) the number of dendritic spines of neurons in each group. Data are reported as mean ± SD. $n = 8$ in each group. #$p < 0.05$ vs Con group; *$p < 0.05$ vs VaD group, one-way ANOVA.

AZ significantly improved the morphology and structure of hippocampal neurons and dendritic remodeling (length and number of dendritic spines) of pyramidal cells in VaD rats

The most common cause of VaD is cerebral ischemia due to cerebrovascular or cardiovascular diseases resulting in a series of neurological, learning, memory disorders and behavioral changes. While the hippocampal region of the brain is extremely sensitive to ischemia, an intact hippocampus is necessary for acquiring spatial information, and deformation or absence of hippocampal tissue is closely related to spatial memory and learning disabilities (Kim et al., 2013; Miyake et al., 2020). Therefore, we performed H&E staining of hippocampal tissue to observe the effect of AZ on neuronal damage. As shown in Fig. 2A, compared with the control group, hippocampal neuronal cells in the VaD group showed dispersed arrangement, cell swelling, significant reduction in number, and widening of the cell gap, suggesting neuronal injury in VaD rats. AZ or mNGF treatment significantly attenuated the above pathologic alterations, and the improvement of hippocampal neuronal morphology and activity was significantly enhanced with a significant increase in pyramidal cell density.

Dendritic spines are the earliest indicators of neuronal excitability and ischemic state. Studies have shown that the decrease or loss of dendritic spine density is closely related to the decline of learning memory function (Brown et al., 2010). Therefore, we used Golgi staining to observe the changes in dendritic spines to further assess the effect of AZ on neuronal damage (Fig. 2C). The dendritic spines of rat hippocampal neurons in the normal group were regular in morphology, neatly arranged, and densely distributed; the dendritic length (Fig. 2D) and the number of dendritic spines of neurons (Fig. 2E)in the model group were significantly reduced, and even broken, with the cytoplasmic gap enlarged; AZ dose-dependently restored the synaptic structure, which resulted in the neuron morphology tending to regularity, and had a significant restorative effect. These histological results were consistent with our observations in animal behavioral experiments.

AZ ameliorates mitochondrial damage induced by oxidative stress

Oxidative stress is a key feature of cerebral ischemic diseases and plays an important role in the pathogenesis of VaD. Some studies have shown that reducing oxidative stress injury has a neuroprotective effect on vascular dementia (Du et al., 2018). We examined some typical oxidative stress parameters, including GSH, MDA, NADPH levels and SOD activity in peripheral blood serum of rats from all groups. The results showed that MDA levels were significantly higher and GSH levels, NADPH, and SOD activities were significantly lower in the VaD group compared to the control group, indicating that oxidative stress injury was present in the rats of the VaD group (Fig. 3A). Although not completely reversed in the AZ intervention group compared to the control group, there was a statistically significant increase in the high-dose AZ group (25 mg kg^{-1}/d) compared to the VaD group, which

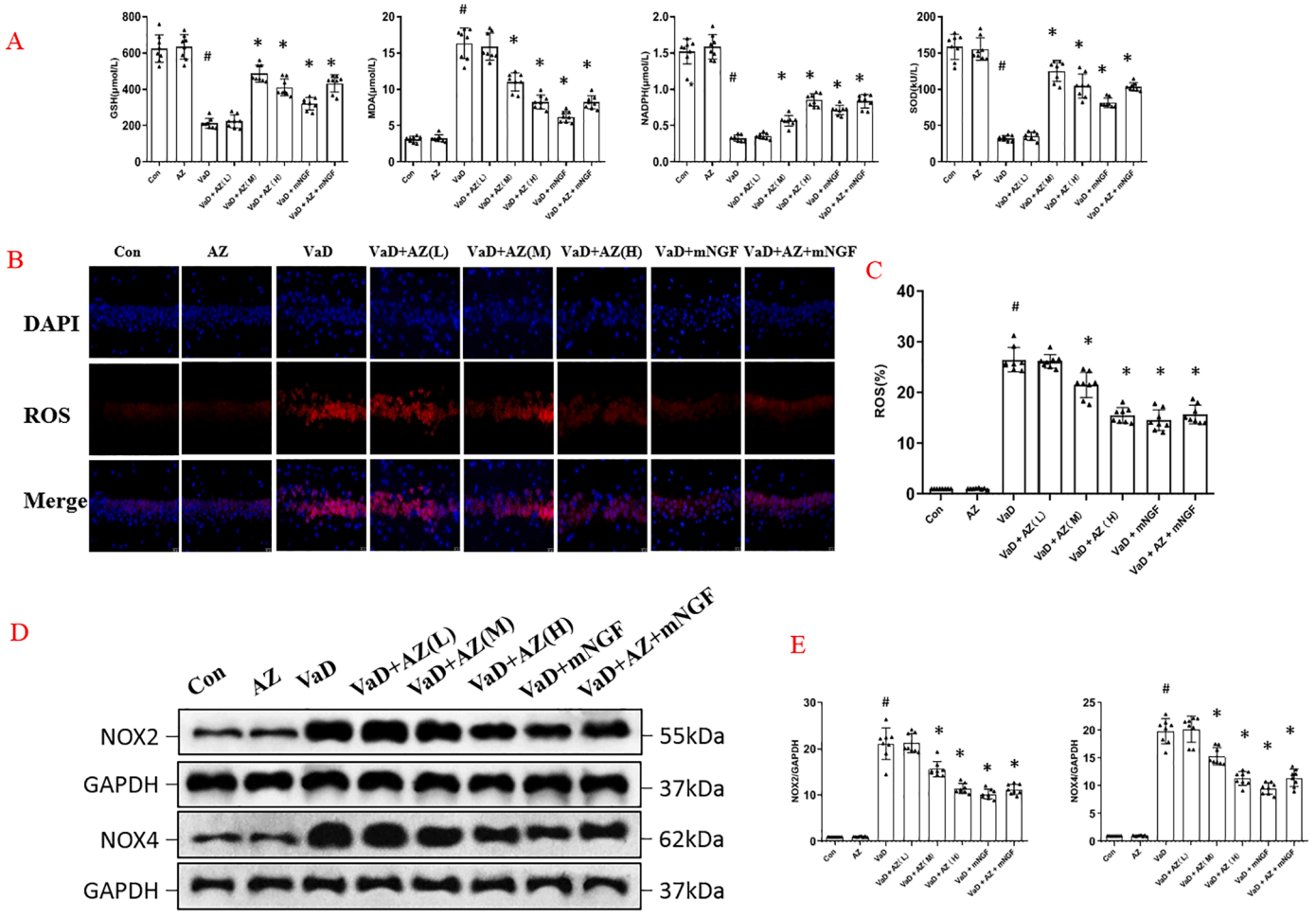

Fig. 3. The antioxidant effect of AZ in VD rats. (A) oxidative stress parameters, including GSH, MDA, NADPH levels and SOD activity in peripheral blood serum of rats from all groups. (B) The content of ROS in hippocampal tissues of rats in each group was detected using DHE fluorescent probe and (C) its statistical analysis. (D) Representative western blots images of NOX2 and NOX4 expression in hippocampal tissues of each group and (E) corresponding quantitative data. Data are reported as mean ± SD. $n = 8$ in each group. #$p < 0.05$ vs Con group; *$p < 0.05$ vs VaD group, one-way ANOVA.

may be related to the sampling site, and oxidative stress parameters in the hippocampal region of the brain may be more meaningful. In view of this, we examined ROS levels in hippocampal tissues using the fluorescent probe DHE, and the results showed that high-dose AZ significantly reversed excessive ROS in the hippocampal region of VaD-injured rats ($p < 0.05$) (Fig. 3B-C). Since NADPH oxidase (NOX) is the main source of ROS in cells, it was significantly increased in ischemic and hypoxic brain (Choi and Lee, 2017; Gao et al., 2012). We also examined NOX2 and NOX4 in the hippocampus, and the expression of NOX2 and NOX4 was significantly increased in the hippocampus of rats in the VaD group, which was consistent with the significantly increased ROS levels. In contrast, high dose of AZ down-regulated the excessive NOX2 and NOX4 expression, and the difference was statistically significant (Fig. 3D-E). The above results consistently confirmed the role of AZ in attenuating oxidative stress injury in VaD rats.

Studies have shown that inadequate cerebral perfusion is also associated with mitochondrial dysfunction, which is considered an early sign of neurodegenerative diseases (e.g., AD) (Bhatia et al., 2022; Esteras et al., 2016). We next assessed the effects of AZ on mitochondrial morphology and function. Transmission electron microscopy showed that the mitochondrial cristae of control neurons were well defined, well bordered, and well aligned, and no obvious mitochondrial swelling was observed. However, in the VaD model group, partial dissolution of mitochondria, obvious swelling, unclear boundaries, disordered arrangement, and obvious mitochondrial morphology abnormalities could be observed. After AZ treatment, mitochondrial swelling was significantly improved, and mitochondrial morphology was partially restored (Fig. 4A-B).

Mitochondrial dynamin-related protein 1 (Drp1) is a key protein that regulates mitochondrial division. Studies have shown that activation of Drp1 leads to mitochondrial damage such as increased mitochondrial division and increased ROS accumulation (Zeng et al., 2022); whereas mitochondrial fission protein 1 (FIS1) is involved in mitochondrial division and plays an important role in maintaining mitochondrial density and preventing mitochondrial swelling (Haileselassie et al., 2019). We analyzed the protein expression of Drp1 and FIS1 in the hippocampus of rats in each group, and the WB results showed that the expression of Drp1 and FIS1 was significantly increased in the hippocampus of rats in the VaD group, which was consistent with the mitochondrial fission damage that we observed in electron microscopy, whereas the AZ decreased the protein expression of Drp1 and FIS1, which may be one of the potential molecular mechanisms by which the AZ can attenuate the structural damage and functional impairment of mitochondria that remains to be investigated (Fig. 4C-D).

In addition, JC-1 detected the mitochondrial membrane potential of neurons in the hippocampal region, and found that the aggregated JC-1

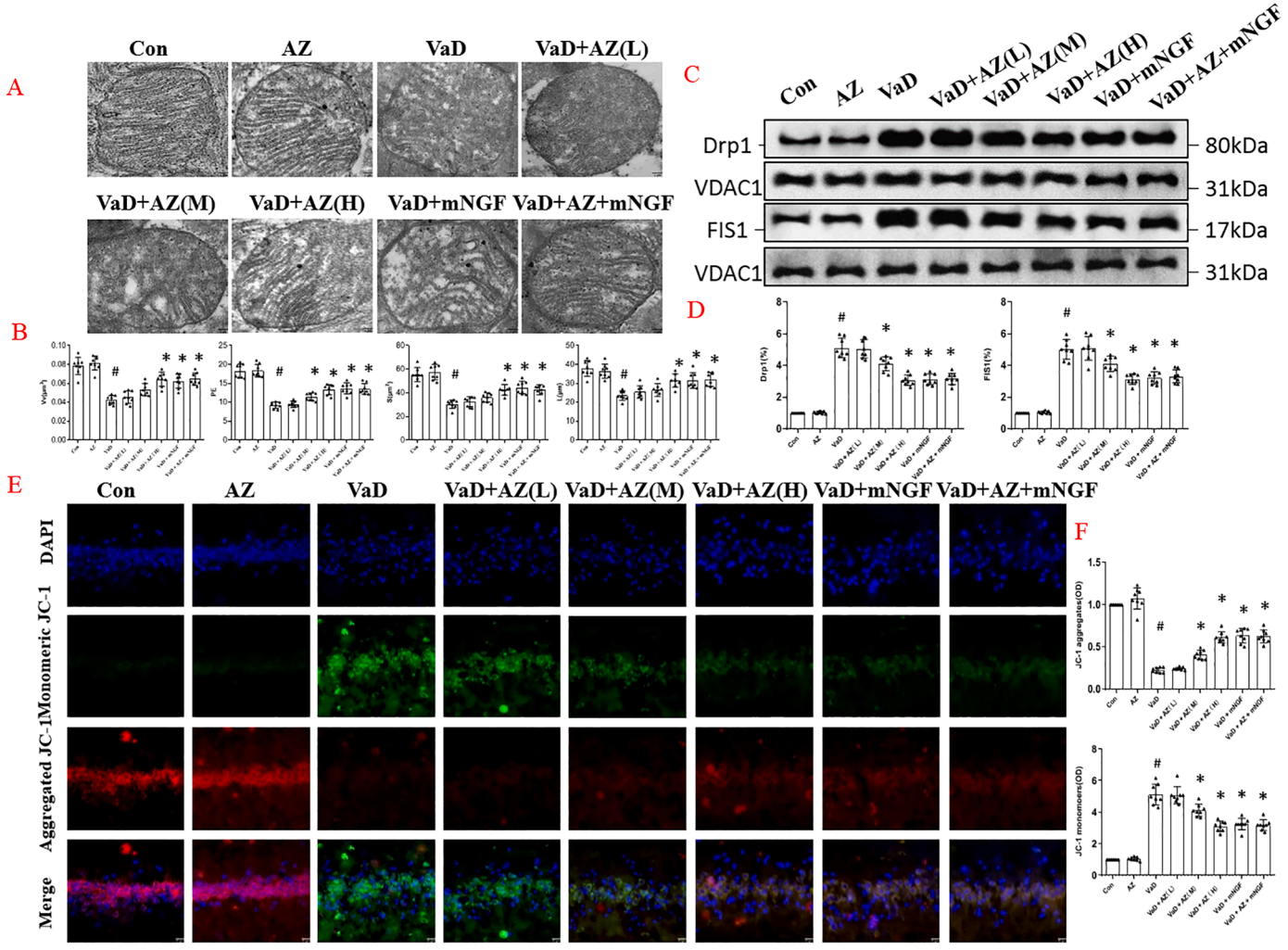

Fig. 4. AZ ameliorates mitochondrial damage in VaD rats. (A) Mitochondrial transmission electron microscope. (B) The quantitative analysis of mitochondrial structure. (C) Representative western blots images of Drp1 and FIS1 expression in hippocampal tissues of each group and (D) corresponding quantitative data. (E) Representation of mitochondrial membrane potential measured by JC-1. (F) Quantitative analysis of aggregated JC-1 and monomeric JC-1. Data are reported as mean ± SD. $n = 8$ in each group. #$p < 0.05$ vs Con group; *$p < 0.05$ vs VaD group, one-way ANOVA.

was significantly reduced while the monomeric type was increased in the VaD-injured rats, suggesting that the mitochondrial membrane potential was significantly decreased in the rats of the VaD group, and it was also a signal for the early stage of cell apoptosis. High-dose AZ has the effect of maintaining mitochondrial membrane potential comparable to that of mNGF (Fig. 4E-F), which also confirms that AZ counteracts VaD-induced mitochondrial dysfunction and the resultant apoptosis, and thus improves cognitive dysfunction in VaD.

AZ reduces TRPM2 expression and JAK1-STAT2 pathway expression in VaD rats

TRPM2 is an effector of oxidative stress, may be a key player in cell death signaling (Hecquet and Malik, 2009). In the central nervous system, the JAK/STAT pathway is involved in a variety of factors that contribute to normal physiological functions, such as cell proliferation, neuronal development, and cell survival, and dysregulation of this pathway can lead to disorders such as cancer, inflammation, and neurodegenerative injury (Lashgari et al., 2021). We examined the expression of TRPM2 and JAK/STAT pathway in various groups of rats by immunofluorescence and western blot, respectively. As shown in Fig. 5A-D, TRPM2 expression was significantly increased in the VaD-injured group compared with the control group, and high-dose AZ decreased the expression of TRPM2 after VaD injury with statistically significant difference. The expression of JAK1 was similar to that of TRPM2, and JAK1 expression was increased in the VaD-injured group, and decreased after high-dose AZ treatment. We examined the different isoforms of STAT, and it was somehow surprising that the expression of STAT2 in the VaD injury group was activated, not STAT1 and STAT3 which were more reported, while medium and high dose AZ reduced STAT2 expression, and the difference was statistically significant compared with VaD injury group.

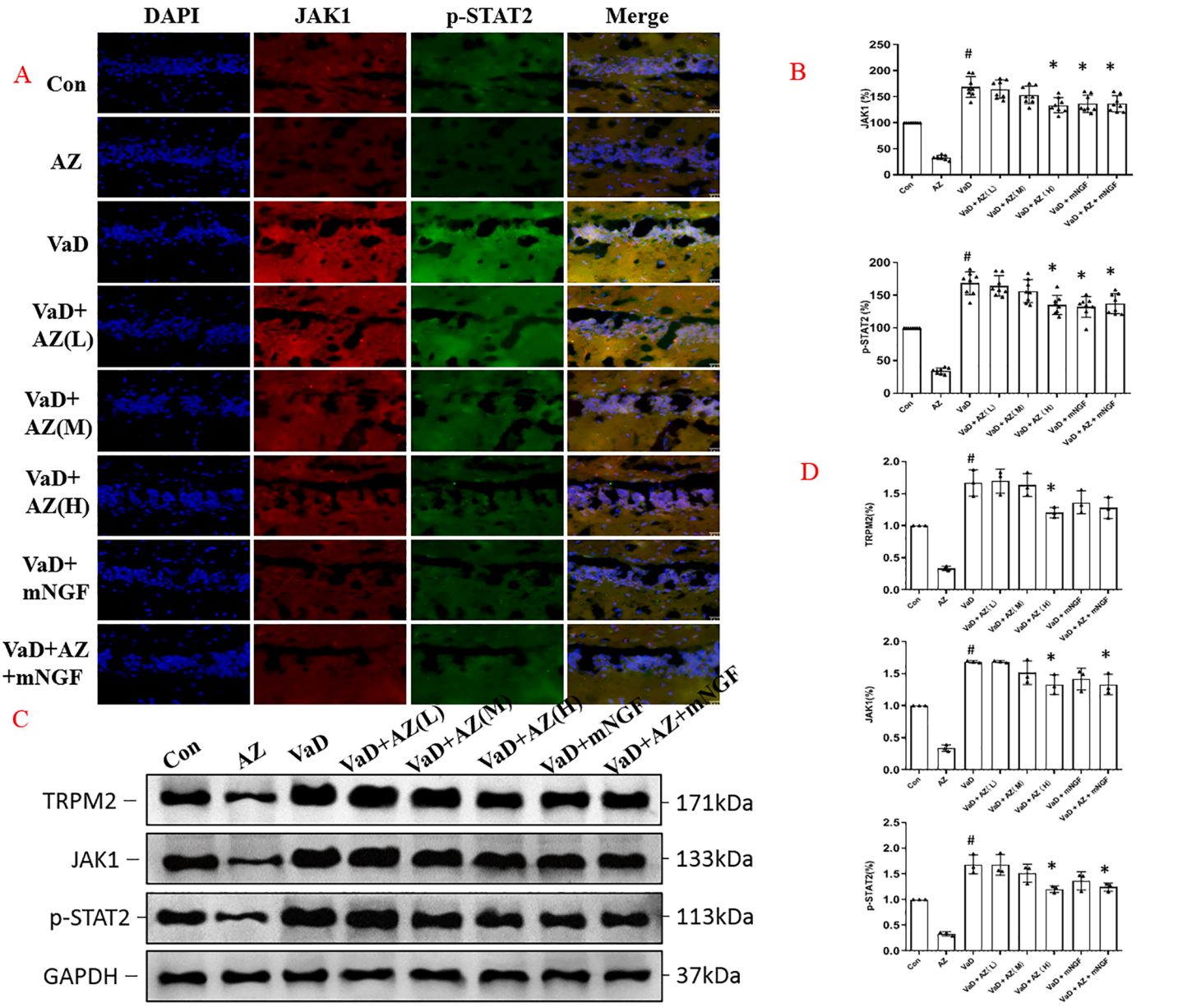

Fig. 5. Effects of AZ on PRPM2 and JAK1-STAT2 pathway expression in VaD rats.
(A)Immunohistochemistry images of JAK1and p-STAT2 in VaD rats of each group. (B) Quantitative data of the positive expression of JAK1and p-STAT2. (C) Representative western blots of the PRPM2, JAK1 and p-STAT2 expression. (D) Statistical analysis of the protein expression of PRPM2, JAK1 and p-STAT2. Data were mean ± SD. #$p < 0.05$ vs Con group; *$p < 0.05$ vs VaD group, one-way ANOVA ($n = 8$ for panels A; $n = 3$ for C).

TRPM2 may be the key target for the AZ

TRPM2 channels may be central to the integration of oxidative stress, dysregulation of calcium regulation and mitochondrial dysfunction, among others (Freestone et al., 2009). To further characterize the functional role of TRPM2 in AZ effects, we performed TRPM2 gene silencing in primary neurons and immunofluorescence and western blot results showed that TRPM2 gene silencing attenuated AZ inhibition of TRPM2; TRPM2 gene silencing also attenuated AZ-induced inhibition of JAK1 and STAT2 expression (Fig. 6A-B). To further confirm the role of TRPM2 in the amelioration of VaD by AZ, we looked at the effect of AZ in TRPM2 knockout mice and observed that TRPM2 knockout similarly attenuated AZ-induced inhibition of JAK1 and STAT2 expression (Fig. 6C-D). These results suggest that TRPM2 may be a key target for AZ to exert ameliorative VaD effects.

TRPM2 binds to Smurf2, leading to ubiquitinated degradation of TRPM2

It has been reported that ubiquitination may play an important role in the regulation of TRPM2 protein levels and activity. Through database exploration, we found that the level of the E3 ubiquitin ligase Smurf2 was negatively correlated with the level of TRPM2. Further, we found that endogenous TRPM2 and Smurf2 proteins were immunoprecipitated in primary neurons (Fig. 7A-D).

To determine whether Smurf2 and TRPM2 co-localized, we ectopically expressed Myc- Smurf2 and HA-TRPM2 in primary neuronal cells and analyzed subcellular localization using immunofluorescence staining. We found that Myc- Smurf2 and HA-TRPM2 co-localized in the cytoplasmic lysate and nucleus as expected (Fig. 7I). These results tentatively suggested that there might be some mechanistic link between Smurf2 and TRPM2, such as ubiquitination degradation of TRPM2 by Smurf2.

Next, we investigated the effect of Smurf2 on TRPM2 ubiquitination. In the presence of MG132, HA-TRPM2 was co-transfected into primary mouse neurons with FLAG ubiquitin and Myc-Smurf2, and the ubiquitinated proteins were immunoprecipitated with anti-HA antibody, and immunoblotted with an anti-Flag antibody to detect ubiquitinated TRPM2. Increased accumulation of ubiquitinated HA-TRPM2 was detected, and Myc-Smurf2 promoted ubiquitination of HA-TRPM2 (Fig. 7E). In addition, we transfected HA-TRPM2, His ubiquitin, and Myc-Smurf2 into mouse primary neurons in the presence of MG132, and then His-tags pulled down the ubiquitinated proteins. HA blotting showed that Smurf2 greatly increased the ubiquitination of HA-TRPM2 (Fig. 7F). Our results suggested that Smurf2 acts as an E3 ligase of TRPM2 to ubiquitinate and degrade proteasomes.

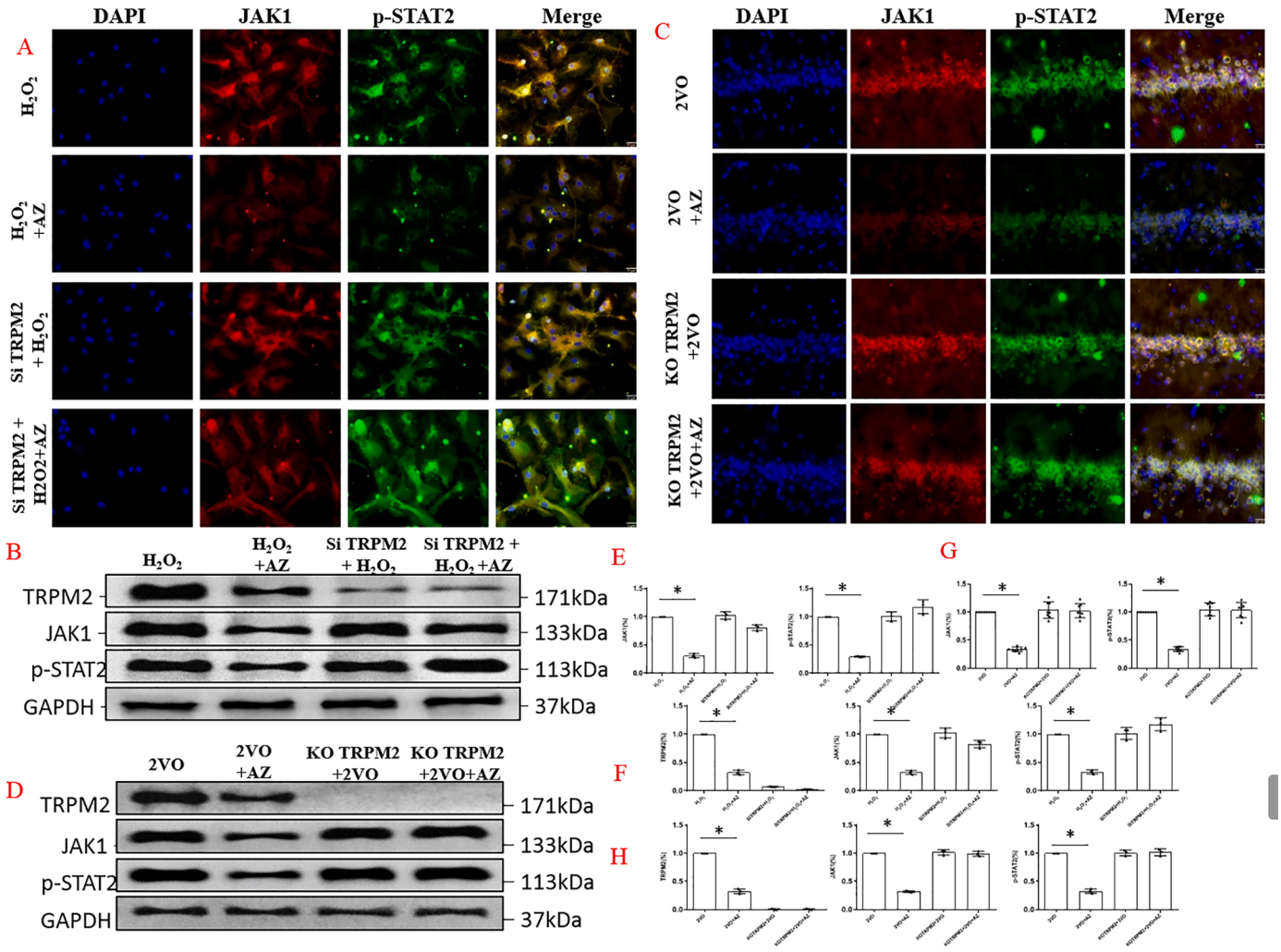

Fig. 6. TRPM2 may be the key target for the effect of AZ. (A and B) JAK1 and p-STAT2 expression in TRPM2 gene silenced primary neurons using immunofluorescence and western blot. (C and D) JAK1 and p-STAT2 expression in TRPM2 knockout mice using immunofluorescence and western blot. (E-F) Statistical analysis for A and B. (G-H) Statistical analysis for C and D. Data were mean ± SD. one-way ANOVA ($n = 8$ for panels C; $n = 3$ for A, B, D).

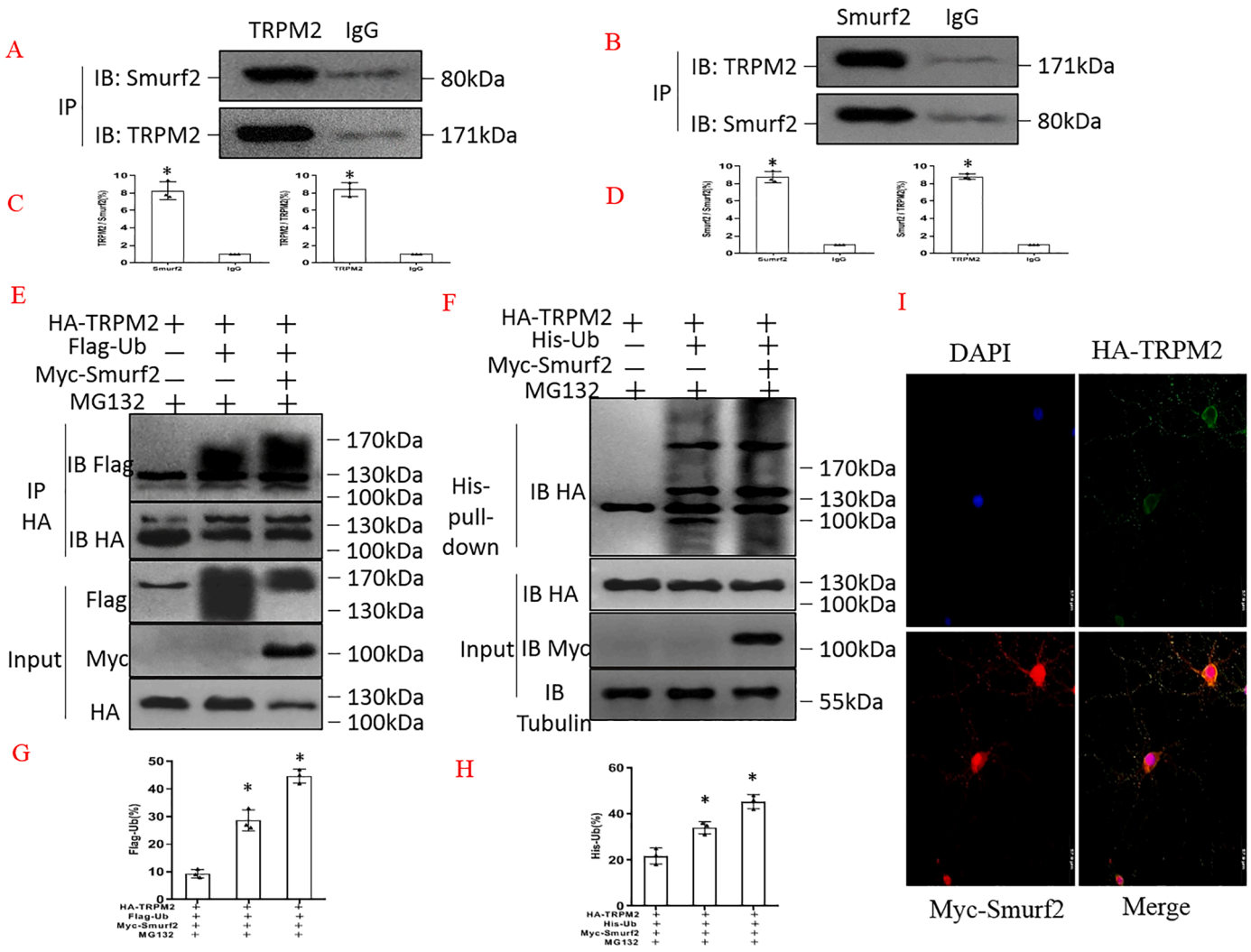

Fig. 7. Smurf2 co-immunoprecipitated with PRPM2 and promoted PRPM2 ubiquitination and proteasomal degradation.
(A-B) co-immunoprecipitation analysis for endogenous Smurf2 and PRPM2 in primary neuronal cells. (C-D) Quantitative analysis of A and B. (E) Smurf2 promoted ubiquitination (Ub) of PRPM2. (F) Smurf2 promoted ubiquitination of PRPM2. (G-H) Quantitative analysis of E and F. (I) ectopically expressed Myc-Smurf2 and HA-PRPM2 co-localized in primary neuronal cells. Red, Myc-Smurf2; green, HA-PRPM2; blue, DAPI. Data were mean ± SD. *, $p < 0.05$, one-way ANOVA. IB, immunoblotting; IP, immunoprecipitation.

MG132 attenuated the effect of AZ, which proved that AZ acted through ubiquitination to degrade TRPM2

Finally, we validated the interaction between Smurf2 and TRPM2. We examined the expression of Smurf2 and TRPM2 in TRPM2$^{+/+}$ VaD rats and H_2O_2-induced injury neurons, respectively. As shown in Fig. 8A and B, the results verified that the expression of Smurf2 was always negatively correlated with the level of TRPM2, both at the animal and cellular levels; whereas high doses of AZ increased the expression of Smurf2 and decreased the expression of TRPM2, with a statistically significant difference. The proteasome inhibitor MG132 decreased Smurf2 expression with a concomitant increase in TRPM2 expression, suggesting that TRPM2 is ubiquitinated and proteasomically degraded (at least partially) via Smurf2 (Fig. 8B), whereas AZ down-regulated TRPM2 expression, as well as the JAK1/STAT2 pathway, by potentiating the action of Smurf2 E3 ubiquitin ligase, thus exerting an attenuating effect on oxidative stress damage.

Discussion

We have previously found that AZ substantially attenuated oxidative stress and improved cardiac dysfunction in rats with diabetic cardiomyopathy (Zhu et al., 2023). In the present study, we focused on the role of AZ in a model of VaD, which is closely related to oxidative stress and its potential specific molecular mechanisms. In this study, we provided strong evidence that AZ improved the morphology and structure of hippocampal neurons in VaD rats, thereby improving spatial learning and memory functions. Consistent with previous findings, AZ reduced oxidative stress levels, improved mitochondrial morphology and function, and maintained the mitochondrial membrane potential, thereby ameliorating cognitive dysfunction in VaD. These independent observations suggest that AZ is a promising candidate for the treatment of VaD.

High and sustained ROS levels impair mitochondrial function, promote hypoxia, and cause cell death (Venkat et al., 2015). Moreover, abnormal mitochondrial morphology and function lead to the failure of the electron transport chain and oxidative phosphorylation, which in turn generates excess ROS (Raz et al., 2010; Toyama et al., 2014) and exacerbates damage. In addition, oxidative stress stimulates the formation of intracellular ADP-ribose through the generation of oxygen metabolites, including H_2O_2, which in turn opens TRPM2 channels. Activated TRPM2 acts as an endogenous redox sensor, causing a sustained increase in the intracellular calcium ion concentration ([Ca^{2+}]i) and activation of the inflammatory response, ultimately inducing cell

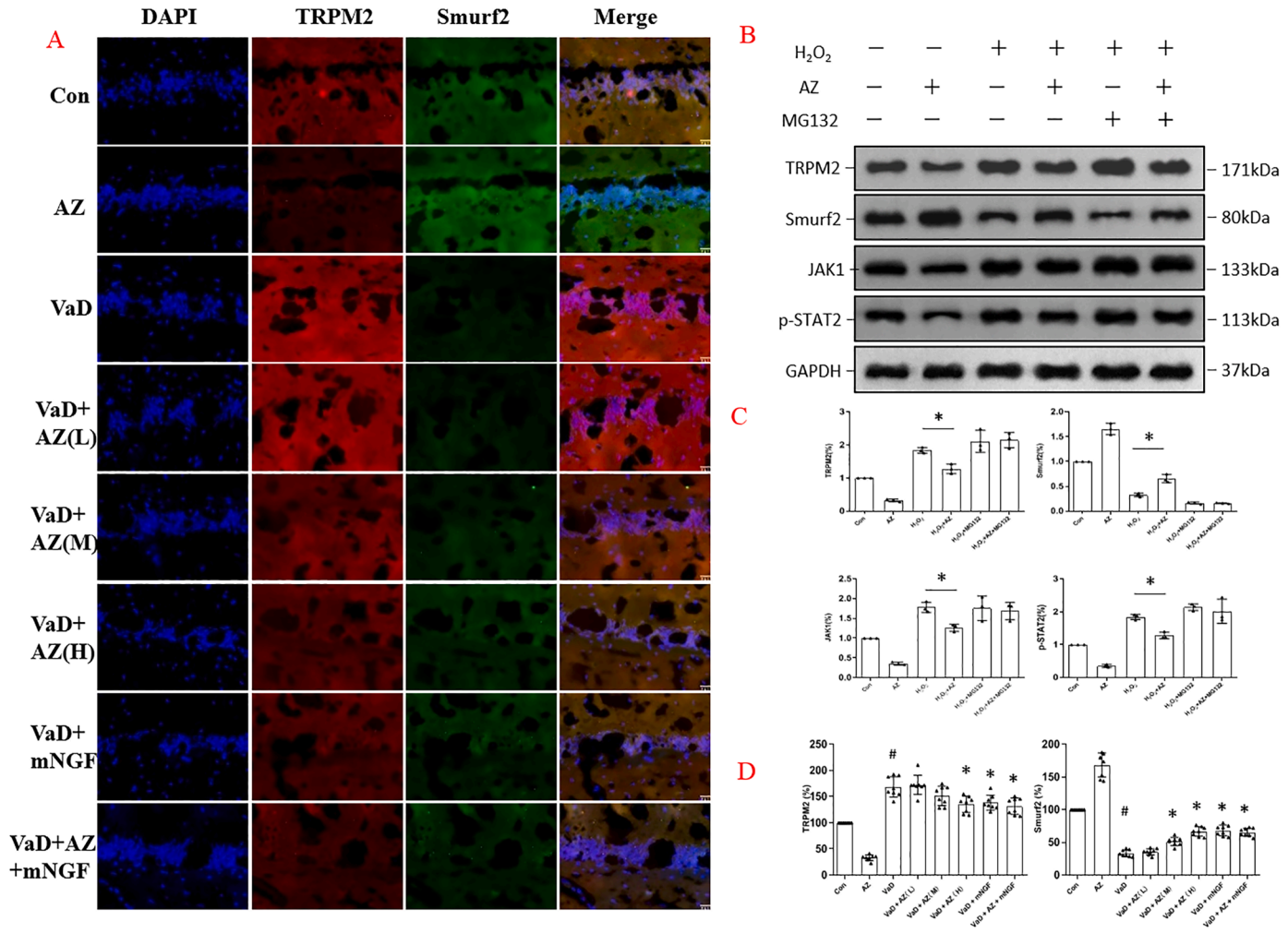

Fig. 8. Smurf2 decreased PRPM2 protein level whereas MG132 blunted Smurf2-induced effects on PRPM2.
(A)Immunohistochemistry images of PRPM2and Smurf2 in VaD rats of each group. (B) Representative western blots of the PRPM2, Smurf2, JAK1 and p-STAT2 expression in H_2O_2-induced injury neurons. (C) Statistical analysis of the protein expression of PRPM2, Smurf2, JAK1 and p-STAT2. (D) Quantitative data of the positive expression of PRPM2 and Smurf2 in VaD rats of each group. $\#p < 0.05$ vs Con group; $^*p < 0.05$ vs VaD group for D. Data were mean ± SD. one-way ANOVA ($n = 8$ for panels A; $n = 3$ for B).

death (Alves-Lopes et al., 2020; Hecquet and Malik, 2009). Conversely, a decrease in channel expression or inhibition of channel function increases cellular resistance to injury. Hiroi et al. found that TRPM2-mediated neutrophil accumulation was associated with the aggravation of myocardial reperfusion injury, and that knockdown of TRPM2 reduced myocardial infarction size after reperfusion (Hiroi et al., 2013). In the present study, we found that the expression of NADPH oxidase was substantially increased in the VaD-injured group compared to that in the control group (Fig. 3D), which was consistent with the increased ROS levels in the hippocampal region of the rats (Fig. 3B). Meanwhile, the expression of Drp1 and FIS1 proteins involved in mitochondrial cleavage damage was also substantially increased (Fig. 4C), which led to instability of the mitochondrial membrane potential and confirmed that oxidative stress and damage to the structure and function of the mitochondria are mutually reinforcing. TRPM2, activated by oxidative stress, is a key molecule that mediates cell damage and death. Our study found that AZ alleviates oxidative stress and improves mitochondrial morphology and function, which may be attributed to a reduction in TRPM2 channel expression or inhibition of its function, revealing for the first time that TRPM2 may be a key target for the action of AZ.

Elucidating the mechanisms underlying TRPM2 activation and regulation is of great interest, because TRPM2 is associated with many pathological states caused by oxidative stress. TRPM2 can be regulated by tyrosine phosphorylation, and dephosphorylation of the widely expressed PTPL1 leads to channel inactivation (Zhang et al., 2007). The ubiquitin-proteasome system is the primary pathway for protein degradation and is crucial in eukaryotes (Koch and Yu, 2019). Several studies have predicted and investigated potential ubiquitination sites in TRPM2; however, the relationship between the E3 ubiquitin ligase, Smurf2, and TRPM2 has not yet been reported. Using IP-MS, we found for the first time that the E3 ubiquitin ligase, Smurf2, binds and co-localizes with TRPM2 (Fig. 7A, B, I). Furthermore, our results indicate that Smurf2 greatly promoted the ubiquitination of TRPM2 (Fig. 7E and F). In this study, Smurf2 was identified as an E3 ligase of TRPM2 that reduces TRPM2 protein levels through proteasomal degradation. AZ triggers the increased ubiquitination and degradation of TRPM2 by enhancing the binding between Smurf2 and TRPM2, which may be a potential molecular mechanism underlying its role in ameliorating VaD.

Calcium ions enter cells after TRPM2 activation and trigger the production of inflammatory cytokines (Yamamoto et al., 2008). The JAK/STAT signaling pathway, also known as the cytokine-stimulated signal transduction pathway (Bolli et al., 2003), is activated by inflammatory cytokines. However, few studies have investigated the relationship between TRPM2 and the JAK/STAT pathway. Our study showed that AZ inhibited TRPM2 activation and suppressed JAK1 and

STAT2 phosphorylation. Moreover, the AZ-induced inhibition of JAK1 and STAT2 expression was substantially attenuated in TRPM2 knockdown neurons and TRPM2 knockout mice (Fig. 6A-D). These results tentatively suggest a connection between TRPM2 and the JAK/STAT pathway. Moslehi et al. also showed that TRPM2 activation by hydrogen peroxide induces the activation of a variety of protein kinases, including phosphatidylinositol 3-kinase (PI3-K), extracellular signal-regulated kinase (ERK) 1/2, JAK2, and p38MAPK (Moslehi and Yazdanparast, 2013). This finding is consistent with our results.

In animal models, JAK/STAT signaling may be involved in mediating cognitive impairment. For example, the inhibition of JAK/STAT signaling by resveratrol alleviated the neuronal deficits and cognitive impairment associated with cerebral ischemia in rats (Chang et al., 2018). However, previous studies have shown that STAT1 and STAT3 have broader biological functions in the central nervous system than the limited effects of STAT2, 4, and 6. For example, STAT1 and STAT3 activate microglia, induce NOX, and increase the formation of ROS and nitric oxide (NO), leading to degeneration of dopamine neurons (Tiwari and Pal, 2017). In addition, JAK activation phosphorylates STAT3 in astrocytes and microglia, which is associated with mitochondrial damage, apoptosis, neuroinflammation, reactive astrocytic proliferation, and genetic mutations (Khera et al., 2022). Previous studies reported that STAT2 is critical for antiviral and immune response modulation (Park et al., 2000; Wang et al., 2021). However, we unexpectedly found a considerable increase in STAT2 phosphorylation in the VaD injury group, suggesting that STAT2 functions in ischemic disease. Consistent with this, studies have underscored the prominent role of STAT2 in regulating mitochondrial homeostasis (Dasgupta et al., 2015; Shahni et al., 2015) and have implicated it as an orchestrator of mitochondrial function and energy production (Dasgupta et al., 2015). STAT2 activation promotes the phosphorylation of Drp1, which contributes to mitochondrial translocation and fission and may lead to lower ATP synthesis and increased electron leakage, which serves as the major source of mitochondrial ROS (Indo et al., 2007). This increasing evidence suggests that STAT2 plays a role in oxidative stress injury, and targeting STAT2 might be a novel strategy for ischemic diseases. We believe that it would be interesting and important to characterize the exact role of STAT2 in VaD and the mechanism by which AZ inhibits STAT2 phosphorylation.

Additionally, it must be acknowledged that despite the construction of animal models of VaD using Sprague-Dawley rats and c57 mice, the mouse VaD model only focused on the validation of the mechanism, lacking behavioral re-observation and verification. Further verification in humans is necessary to detect if AZ has a more definitive role.

In conclusion, we demonstrated that AZ can reduce the oxidative stress level and the resulting mitochondrial damage in VaD rats, improve the morphology and structure of neurons in VaD rats, and boost their spatial learning and memory functions. Thus, AZ is an effective candidate drug for the management of VaD. In terms of the mechanism, it was revealed that TRPM2 may be a key target for the action of AZ, and Smurf2 was identified as the E3 ligase of TRPM2 for the first time. AZ played a role in alleviating oxidative stress damage and improving cognitive dysfunction in VaD rats by enhancing the binding between Smurf2 and TRPM2 and increasing the ubiquitination and degradation levels of TRPM2 (Fig. 9). Although AZ has been used to treat a variety of

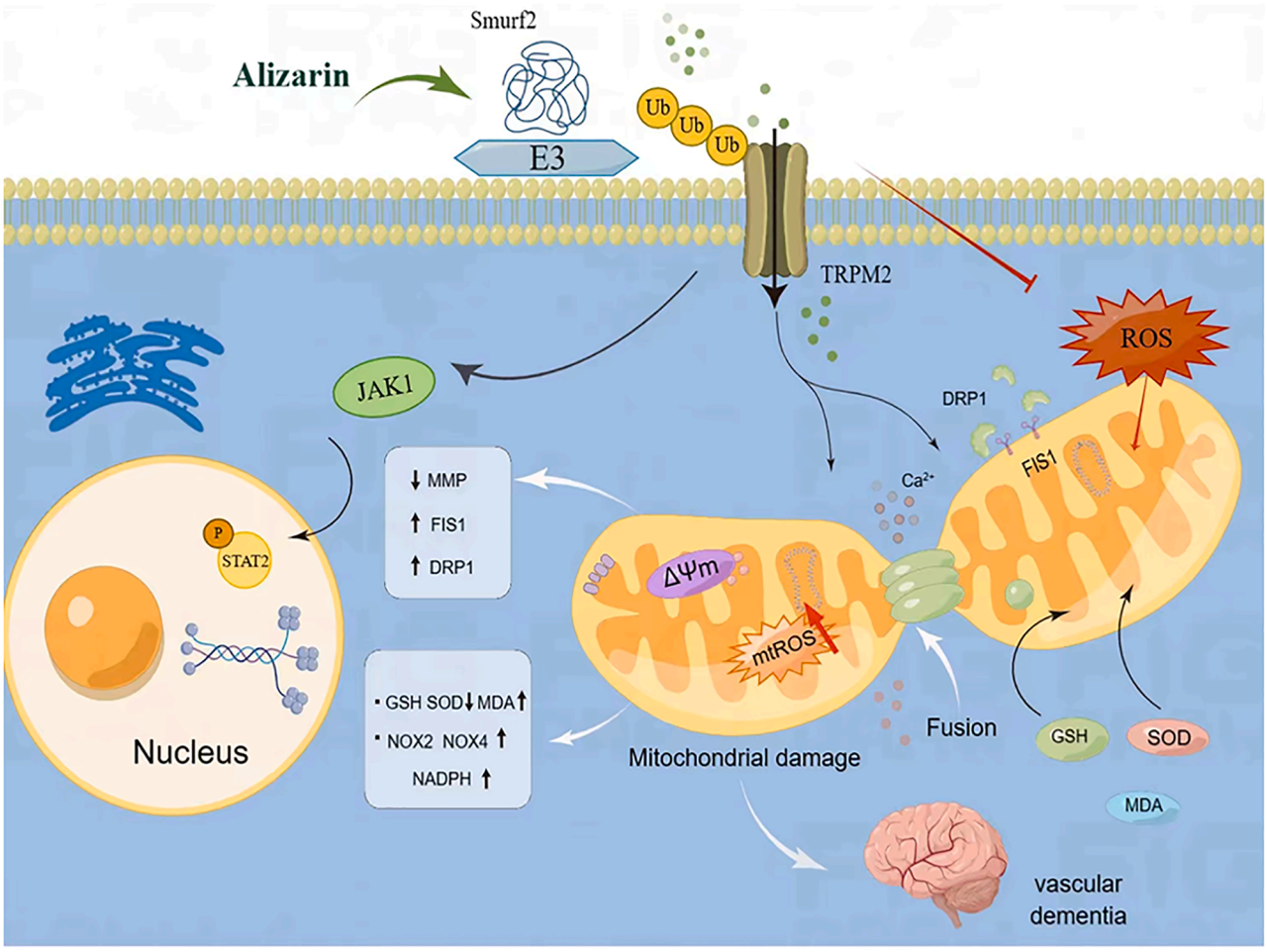

Fig. 9. Alizarin attenuates oxidative stress-induced mitochondrial damage in vascular dementia rats by promoting TRPM2 ubiquitination and proteasomal degradation via Smurf2.

diseases, the effect of AZ on VaD has not been explored. In this study, we clarified, for the first time, the remarkable therapeutic effect of AZ in improving cognitive dysfunction in VaD and elucidated the key targets and degradation pathways of its action, providing strong evidence for the clinical therapeutic effect of AZ in VaD. Given these independent and encouraging observations, we consider AZ as a promising candidate for a novel class of neuroprotectants that may be used as an alternative to currently approved VaD therapies.

Ethics approval and consent to participate

Animal handlings were in accordance with the Guide for Care and Use of Laboratory Animals (NIH, 1996). All methods used were reported in accordance with the ARRIVE guidelines (https://arriveguidelines.org).

Consent for publication

Not applicable.

Availability of data and materials

The data that support the findings of this study are available from the corresponding author upon reasonable request.

Funding

This work was supported by National Natural Science Foundation of China (82271460), Henan Provincial Natural Science Foundation Outstanding Youth Science Fund (242300421025), National High-End Foreign Expert Recruitment Plan of China (G2022026006L), Research Foundation of Xinxiang Medical University (XYBSKYZZ505319).

CRediT authorship contribution statement

Guo-pin Pan: Writing – review & editing, Writing – original draft, Formal analysis, Data curation. **Yan-hua Liu:** Project administration, Methodology. **Ming-xu Qi:** Methodology. **Ya-qi Guo:** Project administration, Methodology. **Zhen-lei Shao:** Methodology. **Hui-ting Liu:** Methodology. **Yi-wen Qian:** Methodology. **Shuang Guo:** Methodology, Data curation. **Ya-ling Yin:** Writing – review & editing, Visualization, Conceptualization. **Peng Li:** Writing – review & editing, Visualization, Supervision, Conceptualization.

Declaration of competing interest

The authors declare that they have no known competing financial interests or personal relationships that could have appeared to influence the work reported in this paper.

Acknowledgements

The authors thank Professor Jiang Lin-Hua for the gift of animals.

Supplementary materials

Supplementary material associated with this article can be found, in the online version, at doi:10.1016/j.phymed.2024.156119.

References

Adhikary, S., Sanyal, S., Basu, M., Sengupta, I., Sen, S., Srivastava, D.K., Roy, S., Das, C., 2016. Selective recognition of H3.1K36 Dimethylation/H4K16 acetylation facilitates the regulation of all-trans-retinoic acid (ATRA)-responsive genes by putative chromatin reader ZMYND8. J. Biol. Chem. 291, 2664–2681.

Alves-Lopes, R., Neves, K.B., Anagnostopoulou, A., Rios, F.J., Lacchini, S., Montezano, A. C., Touyz, R.M., 2020. Crosstalk between vascular redox and calcium signaling in hypertension involves TRPM2 (transient receptor potential Melastatin 2) cation channel. Hypertension 75, 139–149.

Bai, J.Z., Lipski, J., 2010. Differential expression of TRPM2 and TRPV4 channels and their potential role in oxidative stress-induced cell death in organotypic hippocampal culture. Neurotoxicology. 31, 204–214.

Bennett, S., Grant, M.M., Aldred, S., 2009. Oxidative stress in vascular dementia and Alzheimer's disease: a common pathology. J. Alzheimers. Dis. 17, 245–257.

Bhatia, S., Rawal, R., Sharma, P., Singh, T., Singh, M., Singh, V., 2022. Mitochondrial dysfunction in Alzheimer's disease: opportunities for drug development. Curr. Neuropharmacol. 20, 675–692.

Bolli, R., Dawn, B., Xuan, Y.T., 2003. Role of the JAK-STAT pathway in protection against myocardial ischemia/reperfusion injury. Trends. Cardiovasc. Med. 13, 72–79.

Bordet, R., Ihl, R., Korczyn, A.D., Lanza, G., Jansa, J., Hoerr, R., Guekht, A., 2017. Towards the concept of disease-modifier in post-stroke or vascular cognitive impairment: a consensus report. BMC. Med. 15, 107.

Brown, C.E., Boyd, J.D., Murphy, T.H., 2010. Longitudinal in vivo imaging reveals balanced and branch-specific remodeling of mature cortical pyramidal dendritic arbors after stroke. J. Cereb. Blood Flow Metab. 30, 783–791.

Cai, Y., Luo, Q., Sun, M., Corke, H., 2004. Antioxidant activity and phenolic compounds of 112 traditional Chinese medicinal plants associated with anticancer. Life Sci. 74, 2157–2184.

Cai, Y.Z., Mei, S., Jie, X., Luo, Q., Corke, H., 2006. Structure-radical scavenging activity relationships of phenolic compounds from traditional Chinese medicinal plants. Life Sci. 78, 2872–2888.

Chang, C., Zhao, Y., Song, G., She, K., 2018. Resveratrol protects hippocampal neurons against cerebral ischemia-reperfusion injury via modulating JAK/ERK/STAT signaling pathway in rats. J. Neuroimmunol. 315, 9–14.

Choi, D.H., Lee, J., 2017. A Mini-Review of the NADPH oxidases in Vascular Dementia: correlation with NOXs and Risk Factors for VaD. Int. J. Mol. Sci. 18.

Chrissobolis, S., Banfi, B., Sobey, C.G., Faraci, F.M., 2012. Role of Nox isoforms in angiotensin II-induced oxidative stress and endothelial dysfunction in brain. J. Appl. Physiol. 113 (1985), 184–191.

Convertino, M., Pellarin, R., Catto, M., Carotti, A., Caflisch, A., 2009. 9,10-Anthraquinone hinders beta-aggregation: how does a small molecule interfere with Abeta-peptide amyloid fibrillation? Protein Sci. 18, 792–800.

Dasgupta, A., Chen, K.H., Tian, L., Archer, S.L., 2015. Gone fission: an asymptomatic STAT2 mutation elongates mitochondria and causes human disease following viral infection. Brain 138, 2802–2806.

Du, S.Q., Wang, X.R., Zhu, W., Ye, Y., Yang, J.W., Ma, S.M., Ji, C.S., Liu, C.Z., 2018. Acupuncture inhibits TXNIP-associated oxidative stress and inflammation to attenuate cognitive impairment in vascular dementia rats. CNS. Neurosci. Ther. 24, 39–46.

Erkinjuntti, T., Román, G., Gauthier, S., Feldman, H., Rockwood, K., 2004. Emerging therapies for vascular dementia and vascular cognitive impairment. Stroke 35, 1010–1017.

Esteras, N., Dinkova-Kostova, A.T., Abramov, A.Y., 2016. Nrf2 activation in the treatment of neurodegenerative diseases: a focus on its role in mitochondrial bioenergetics and function. Biol. Chem. 397, 383–400.

Finger, C.E., Moreno-Gonzalez, I., Gutierrez, A., Moruno-Manchon, J.F., McCullough, L. D., 2022. Age-related immune alterations and cerebrovascular inflammation. Mol. Psychiatry 27, 803–818.

Fivenson, E.M., Lautrup, S., Sun, N., Scheibye-Knudsen, M., Stevnsner, T., Nilsen, H., Bohr, V.A., Fang, E.F., 2017. Mitophagy in neurodegeneration and aging. Neurochem. Int. 109, 202–209.

Fotia, C., Avnet, S., Granchi, D., Baldini, N., 2012. The natural compound Alizarin as an osteotropic drug for the treatment of bone tumors. J. Orthop. Res. 30, 1486–1492.

Freestone, P.S., Chung, K.K., Guatteo, E., Mercuri, N.B., Nicholson, L.F., Lipski, J., 2009. Acute action of rotenone on nigral dopaminergic neurons–involvement of reactive oxygen species and disruption of Ca2+ homeostasis. Eur. J. Neurosci. 30, 1849–1859.

Fuentes, M., Araya-Maturana, R., Palomo, I., Fuentes, E., 2018. Platelet mitochondrial dysfunction and mitochondria-targeted quinone-and hydroquinone-derivatives: review on new strategy of antiplatelet activity. Biochem. Pharmacol. 156, 215–222.

Gao, H.M., Zhou, H., Hong, J.S., 2012. NADPH oxidases: novel therapeutic targets for neurodegenerative diseases. Trends. Pharmacol. Sci. 33, 295–303.

Gray, S.P., Jandeleit-Dahm, K.A., 2015. The role of NADPH oxidase in vascular disease–hypertension, atherosclerosis & stroke. Curr. Pharm. Des. 21, 5933–5944.

Haileselassie, B., Mukherjee, R., Joshi, A.U., Napier, B.A., Massis, L.M., Ostberg, N.P., Queliconi, B.B., Monack, D., Bernstein, D., Mochly-Rosen, D., 2019. Drp1/Fis1 interaction mediates mitochondrial dysfunction in septic cardiomyopathy. J. Mol. Cell Cardiol. 130, 160–169.

Hecquet, C.M., Malik, A.B., 2009. Role of H(2)O(2)-activated TRPM2 calcium channel in oxidant-induced endothelial injury. Thromb. Haemost. 101, 619–625.

Hiroi, T., Wajima, T., Negoro, T., Ishii, M., Nakano, Y., Kiuchi, Y., Mori, Y., Shimizu, S., 2013. Neutrophil TRPM2 channels are implicated in the exacerbation of myocardial ischaemia/reperfusion injury. Cardiovasc. Res. 97, 271–281.

Indo, H.P., Davidson, M., Yen, H.C., Suenaga, S., Tomita, K., Nishii, T., Higuchi, M., Koga, Y., Ozawa, T., Majima, H.J., 2007. Evidence of ROS generation by mitochondria in cells with impaired electron transport chain and mitochondrial DNA damage. Mitochondrion. 7, 106–118.

Jeremić, S., Amić, A., Stanojević-Pirković, M., Marković, Z., 2018. Selected anthraquinones as potential free radical scavengers and P-glycoprotein inhibitors. Org. Biomol. Chem. 16, 1890–1902.

Kalaria, R.N., 2018. The pathology and pathophysiology of vascular dementia. Neuropharmacology. 134, 226–239.

Khera, R., Mehan, S., Kumar, S., Sethi, P., Bhalla, S., Prajapati, A., 2022. Role of JAK-STAT and PPAR-Gamma Signalling modulators in the prevention of autism and neurological dysfunctions. Mol. Neurobiol. 59, 3888–3912.
Kim, B.K., Ko, I.G., Kim, S.E., Kim, C.J., Yoon, J.S., Baik, H.H., Jin, B.K., Lee, C.Y., Baek, S.B., Shin, M.S., 2013. Impact of several types of stresses on short-term memory and apoptosis in the hippocampus of rats. Int. Neurourol. J. 17, 114–120.
Koch, B., Yu, H.G., 2019. Regulation of inner nuclear membrane associated protein degradation. Nucleus. 10, 169–180.
Korczyn, A.D., Vakhapova, V., Grinberg, L.T., 2012. Vascular dementia. J. Neurol. Sci. 322, 2–10.
Lanza, G., Cantone, M., Musso, S., Borgione, E., Scuderi, C., Ferri, R., 2018. Early-onset subcortical ischemic vascular dementia in an adult with mtDNA mutation 3316G>A. J. Neurol. 265, 968–969.
Lashgari, N.A., Roudsari, N.M., Momtaz, S., Sathyapalan, T., Abdolghaffari, A.H., Sahebkar, A., 2021. The involvement of JAK/STAT signaling pathway in the treatment of Parkinson's disease. J. Neuroimmunol. 361, 577758.
Li, X., Jiang, L.H., 2019. A critical role of the transient receptor potential melastatin 2 channel in a positive feedback mechanism for reactive oxygen species-induced delayed cell death. J. Cell Physiol. 234, 3647–3660.
Li, Y., Zhang, T., Zhang, X., Zou, W., Gong, X., Fu, J., 2017. Cinepazide maleate improves cognitive function and protects hippocampal neurons in diabetic rats with chronic cerebral hypoperfusion. Biol. Pharm. Bull. 40, 249–255.
Malko, P., Jiang, L.H., 2020. TRPM2 channel-mediated cell death: an important mechanism linking oxidative stress-inducing pathological factors to associated pathological conditions. Redox. Biol. 37, 101755.
Miller, B.A., 2019. TRPM2 in Cancer. Cell Calcium 80, 8–17.
Miyake, K., Yagi, S., Aoki, Y., Shikano, Y., Ikegaya, Y., Sasaki, T., 2020. Acute effects of ethanol on hippocampal spatial representation and offline reactivation. Front. Cell Neurosci. 14, 571175.
Moslehi, M., Yazdanparast, R., 2013. SK-N-MC cell death occurs by distinct molecular mechanisms in response to hydrogen peroxide and superoxide anions: involvements of JAK2-STAT3, JNK, and p38 MAP kinases pathways. Cell Biochem. Biophys. 66, 817–829.
Nam, W., Kim, S.P., Nam, S.H., Friedman, M., 2017. Structure-antioxidative and anti-inflammatory activity relationships of purpurin and related anthraquinones in chemical and cell assays. Molecules. 22.
O'Brien, J.T., Thomas, A., 2015. Vascular dementia. Lancet 386, 1698–1706.
Park, C., Li, S., Cha, E., Schindler, C., 2000. Immune response in Stat2 knockout mice. Immunity. 13, 795–804.
Parodi-Rullán, R., Sone, J.Y., Fossati, S., 2019. Endothelial mitochondrial dysfunction in cerebral amyloid angiopathy and Alzheimer's disease. J. Alzheimers. Dis. 72, 1019–1039.
Qiu, Y., Xue, X.J., Liu, G., Shen, M.M., Chao, C.Y., Zhang, J., Guo, Y.Q., Niu, Q.Q., Yu, Y. N., Song, Y.T., Wang, H.H., Wang, S.X., Chen, Y.J., Jiang, L.H., Li, P., Yin, Y.L., 2021. Perillaldehyde improves cognitive function in vivo and in vitro by inhibiting neuronal damage via blocking TRPM2/NMDAR pathway. Chin. Med. 16, 136.
Ramsey, I.S., Delling, M., Clapham, D.E., 2006. An introduction to TRP channels. Annu. Rev. Physiol. 68, 619–647.
Raz, L., Zhang, Q.G., Zhou, C.F., Han, D., Gulati, P., Yang, L.C., Yang, F., Wang, R.M., Brann, D.W., 2010. Role of Rac1 GTPase in NADPH oxidase activation and cognitive impairment following cerebral ischemia in the rat. PLoS. One 5, e12606.
Romay, M.C., Toro, C., Iruela-Arispe, M.L., 2019. Emerging molecular mechanisms of vascular dementia. Curr. Opin. Hematol. 26, 199–206.
Shahni, R., Cale, C.M., Anderson, G., Osellame, L.D., Hambleton, S., Jacques, T.S., Wedatilake, Y., Taanman, J.W., Chan, E., Qasim, W., Plagnol, V., Chalasani, A., Duchen, M.R., Gilmour, K.C., Rahman, S., 2015. Signal transducer and activator of transcription 2 deficiency is a novel disorder of mitochondrial fission. Brain 138, 2834–2846.
Tiwari, P.C., Pal, R., 2017. The potential role of neuroinflammation and transcription factors in Parkinson disease. Dialogues. Clin. Neurosci. 19, 71–80.
Toyama, K., Koibuchi, N., Uekawa, K., Hasegawa, Y., Kataoka, K., Katayama, T., Sueta, D., Ma, M.J., Nakagawa, T., Yasuda, O., Tomimoto, H., Ichijo, H., Ogawa, H., Kim-Mitsuyama, S., 2014. Apoptosis signal-regulating kinase 1 is a novel target molecule for cognitive impairment induced by chronic cerebral hypoperfusion. Arterioscler. Thromb. Vasc. Biol. 34, 616–625.
Venkat, P., Chopp, M., Chen, J., 2015. Models and mechanisms of vascular dementia. Exp. Neurol. 272, 97–108.
Wang, Y., Song, Q., Huang, W., Lin, Y., Wang, X., Wang, C., Willard, B., Zhao, C., Nan, J., Holvey-Bates, E., Wang, Z., Taylor, D., Yang, J., Stark, G.R., 2021. A virus-induced conformational switch of STAT1-STAT2 dimers boosts antiviral defenses. Cell Res. 31, 206–218.
Warren, C.M., Ziyad, S., Briot, A., Der, A., Iruela-Arispe, M.L., 2014. A ligand-independent VEGFR2 signaling pathway limits angiogenic responses in diabetes. Sci. Signal. 7, ra1.
Xie, Y.F., Macdonald, J.F., Jackson, M.F., 2010. TRPM2, calcium and neurodegenerative diseases. Int. J. Physiol. Pathophysiol. Pharmacol. 2, 95–103.
Xu, Z., Zhu, X., Su, L., Zou, C., Chen, X., Hou, Y., Gong, C., Ng, W., Ni, Z., Wang, L., Yan, X., Zhu, Y., Jiao, X., Yao, C., Zhu, S., 2020. A high-throughput assay for screening natural products that boost NK cell-mediated killing of cancer cells. Pharm. Biol. 58, 357–366.
Yamamoto, S., Shimizu, S., Kiyonaka, S., Takahashi, N., Wajima, T., Hara, Y., Negoro, T., Hiroi, T., Kiuchi, Y., Okada, T., Kaneko, S., Lange, I., Fleig, A., Penner, R., Nishi, M., Takeshima, H., Mori, Y., 2008. TRPM2-mediated Ca2+influx induces chemokine production in monocytes that aggravates inflammatory neutrophil infiltration. Nat. Med. 14, 738–747.
Yang, T., Zhang, F., 2021. Targeting transcription factor Nrf2 (nuclear factor erythroid 2-related factor 2) for the intervention of vascular cognitive impairment and dementia. Arterioscler. Thromb. Vasc. Biol. 41, 97–116.
Yang, Y., Zhao, X., Zhu, Z., Zhang, L., 2022. Vascular dementia: a microglia's perspective. Ageing Res. Rev. 81, 101734.
Yin, Y.L., Liu, Y.H., Zhu, M.L., Wang, H.H., Qiu, Y., Wan, G.R., Li, P., 2022. Floralozone improves cognitive impairment in vascular dementia rats via regulation of TRPM2 and NMDAR signaling pathway. Physiol. Behav. 249, 113777.
Zeng, X., Zhang, Y.D., Ma, R.Y., Chen, Y.J., Xiang, X.M., Hou, D.Y., Li, X.H., Huang, H., Li, T., Duan, C.Y., 2022. Activated Drp1 regulates p62-mediated autophagic flux and aggravates inflammation in cerebral ischemia-reperfusion via the ROS-RIP1/RIP3-exosome axis. Mil. Med. Res. 9, 25.
Zhang, W., Tong, Q., Conrad, K., Wozney, J., Cheung, J.Y., Miller, B.A., 2007. Regulation of TRP channel TRPM2 by the tyrosine phosphatase PTPL1. Am. J. Physiol. Cell Physiol. 292, C1746–C1758.
Zhu, M.L., Yu, Y.N., Song, Y.T., Wang, C.Y., Miao, Z., Chen, B.L., Guo, S., Shen, M.M., Zhang, M.X., Zhan, H.Q., Yang, P.F., Wang, Q.Q., Yin, Y.L., Li, P., 2023. Cardioprotective role of A-cycloglycosylated derivative of Rubiadin in diabetic cardiomyopathy in rats. Int. Immunopharmacol. 118, 110008.
Zielińska, W., Zabrzyński, J., Gagat, M., Grzanka, A., 2021. The role of TRPM2 in endothelial function and dysfunction. Int. J. Mol. Sci. 22.